ANALYSIS OF ZnO-NANORODS GROWN ON *p*-Si (100) VIA CATALYST-FREE HYDROTHERMAL DEPOSITION

Accoc. Prof.Dr.Eng. Oleg Lupan
Technical University of Moldova

INTRODUCTION

The *n*-ZnO nanorod arrays/*p*-Si heterojunction for photo-detector structures was fabricated by a rapid hydrothermal deposition without employing a catalyst or seed layer. X-ray diffraction spectra showed that ZnO nanorod arrays were grown with *c*-axis relationship to the *p*-Si substrate. The photodetection mechanism for the *n*-ZnO/*p*-Si heterostructure is discussed.

1. ZnO-NANOROD - BASED OPTOELECTRONIC DEVICES

Zinc oxide (ZnO) is an attractive material since it has both a direct band gap (of ~3.4 eV) and a very large free exciton binding energy (of ~60 meV) [1]. Zinc oxide nanorods (ZnO NRs) are most promising one-dimensional nanostructures which present enormous interest for low-dimensional light emitters or photodetectors in various nanophotonics systems [2]. It is due to their unique physical and chemical properties, which should favor light emission at room temperature [3]. At the same time, small-diameter ZnO nanowires are expected to lower the lasing threshold because quantum effects result in enhancement of density of states near the band edges and radiative recombination due to carrier confinement [4]. Since the reported room-temperature lasing actions of ZnO nanorod arrays [5], a diversity of scientific research was undertaken reported on zinc oxide for use in short-wavelength optoelectronic devices ensuring efficient utilization in applications [6-8].

In this context multiple device structures, such as heterojunction [9], homojunction [10], or metal-insulator-semiconductor structure [11], have been explored to generate the UV and visible electro-luminescence from zinc oxide. Liu *et al*. [12] investigated the effects of post-annealing on the electrical properties of *n*-ZnO/*p*-Si heterojunction obtained by hydrothermal technique by using a ZnO seed layer deposited by ion beam sputtering technique. The large difference in the thermal expansion coefficients of the two materials [13] and the high reactivity of Si is problematic for producing ZnO/Si heterojunctions by conventional thermal processing. According to Kayes *et al*. [14] it has been demonstrated theoretically and experimentally that nanorod semiconductor arrays arranged perpendicular to the substrate enhance the overall efficiency. The ZnO/Si system is interesting due to the fundamental information it may provide about synthesis and heteroepitaxy in large mismatch systems (>40%), which could be useful for producing efficient devices. To overcome such problems different techniques for surface pre-treatment have been reported, like deposition of ZnS [15], GaN [16], nitridation of the Si surface [17], CaF_2 [18]. The introduction of the insulating layer (e.g. SiN or CaF_2), will affect the electrical properties of ZnO/Si junction [19-20]. Few studies concerning the growth of catalyst-free ZnO thin films on Si substrates by different techniques have been performed, due to inherent problems encountered in the growth process [19]. Aqueous solution synthesis is known to be a simple, low temperature, and large-area deposition technique for group II-VI semiconductors such as ZnO. Despite reported achievements, data are not good enough to be implemented in on ZnO/Si due to their low efficiency, which still makes this field of great research interest to develop a process for growing ZnO nanorods directly on *n*- and *p*-Si substrates. Also, it is to be taken into account that at this stage, the aqueous chemical synthesis of ZnO nanorods on *n*- and *p*-Si is not extensively studied yet. From another side, silicon substrates come in our research focus, because Si is not only of interest to integration of optoelectronic devices, but also the cheapest wafer materials with a cubic structure [21]. Also, Si is easier to cleave in comparison with other substrates (i.e. GaAs). Considering *n*- and *p*-type Si as the substrate for the fabrication *n*-ZnO/*p*-Si or *n*-ZnO/*n*-Si hetero-junctions by the chemical technique looks more promising for nano-LEDs arrays and photodiodes. To overcome the limited availability of documentation on growth of ZnO nanorods on Si and implement their properties it is necessarily to find optimum regimes for growing nanorods on Si.

Here, we present a detailed cleaning procedure for Si to get deposited ZnO at low temperature (95-98°C). Also, it is reported on hydrothermal technique used to synthesize ZnO nanorod arrays on *p*-Si in 15 min. Their characteristics have been studied and a high quality material was identified by micro-Raman and photoluminescence measurements. Also, the fabricated heterostructures by this method show feasibility as a new optoelectronic device structure.

2. EXPERIMENT DETAILS

The ZnO nanorod arrays were grown on the *p*-type Si (100) substrates with an electrical resistivity 0.05 Ω·cm. We used these substrates because, the crystal orientation of the majority of wafers used today is (100) [22]. Silicon samples are commonly platelets cleaved from a Si wafer and has been sequentially cleaned by using solvent clean step, RCA-1 clean and HF dip as reported before [23]. The most common cleaning procedure for silicon wafers in electronic device manufacturing is the deionized (DI) water rinse. Cleaning processes for silicon surface are performed in water-based solutions, with the exception of solvent (acetone or isopropylalcohol) cleaning step, which are used to remove organic contaminants. Solvent clean step consists in placing Si wafers in the warm acetone bath (50-53°C) for 10 min, and then followed by ultrasonically cleaning in DI for 2-3 min. As acetone leaves its own residues, Si wafers were placed in methanol for 4-5 min under ultrasonical cleaning. After this step the substrates were rinsed abundantly with deionized water (optional), and then blow dry with a flux of air. RCA clean was used to remove organic residues from Si wafers. At this stage silicon is oxidized, in order to leave a thin SiO_2 on the surface of the substrate. The recipe used for RCA-1 [23] cleanser consists of 50 ml DI water, 10 ml of ammonium hydroxide (27%) mixed and heated at 70-75°C on hot plate, then 10 ml of hydrogen peroxide (30% H_2O_2) was added. After 2 minutes of vigorously bubbling of RCA-1 solution, Si wafers was soak in it for 15-20 min. After this step Si wafers were transferred to a beaker with overflowing DI water to rinse and remove the remained solution. Afterwards a hydrophilic surface condition was observed which is related to the presence of a high density of silanol groups (Si–OH) or to a thin interfacial oxide film [21-23]. Afterwards, the oxidized substrates were dipped for 3 min in hydrofluoric acid (2% HF made from 240 ml DI water and 10 ml HF of 49%) in a polypropylene beaker to remove silicon dioxide from the Si surfaces and thoroughly rinsed in running deionized (DI) water (18.2 MΩ·cm) flow. Si wafers showed hydrophobicity observed by realizing wetting test (a little DI water drop on the surface beads up and rolls off – not shown).

Next, samples were dipped in an aqueous solution prepared by using 0.1-0.5 M of zinc sulfate (99.5%) with an ammonia solution of 29.4% (Fisher Scientific). The vessels is placed on a preheated oven for 15 min at 95 °C and then allowed to cool down naturally to room temperature [24]. After the ZnO arrays on the Si were rinsed in DI for 5 min and then the samples were dried in air at 200 °C for 5 min. It is of importance to find an optimum deposition regime for an optimum ZnO/*p*-Si interface formation where a very thin SiO_2 layer is formed after deposition.

The synthesized products were characterized by XRD (Rigaku 'DB/MAX' powder diffractometer) and a scanning electron microscope (SEM). The composition of ZnO nanorods was carried out using the Energy dispersive X-ray spectroscopy (EDX). The room temperature Raman scattering was investigated with a Confocal Laser Raman System in the backscattering geometry under the excitation by a 532 nm laser. Current-voltage (*I-V*) characteristics were measured using a semiconductor parameter analyzer with input impedance of 2.00×10^8 Ω [25]. ZnO/*p*-Si structure was exposed to UV-Vis light in order to investigate spectral response measured with the aid a Xe arc lamp dispersed by a monochromator. The light was modulated with a mechanical chopper.

3. RESULTS AND DISCUSSIONS

The XRD spectrum shown in Figure 1 agreed with the standard card of ZnO with hexagonal structure (JCPDS 036-1451) and no diffraction peaks from of other impurities were detected. The strong intensity and narrow XRD peaks of ZnO are indicative of the good crystallinity of material. The (002) peak at 34.42° was dominant and shows that ZnO nanorods are quasi-oriented and the growth direction was along (001). Presence of other peaks (100), (101), (102), (110), (103) and (112) demonstrate that nonepitaxial growth has performed in our procedure. The lattice constants *a* and *c* of wurtzite structure ZnO were calculated, according to Bragg's law:

$$n\lambda = 2d\sin\theta \qquad (1)$$

where *n* is the order of diffraction (usually *n* =1), λ is the X-ray wavelength and *d* is the spacing between planes of given Miller indices *h*, *k* and *l*.

The lattice constants *a* and *c* were determined as *a* = 0.3250 nm, *c* = 0.5210 nm for pure ZnO.

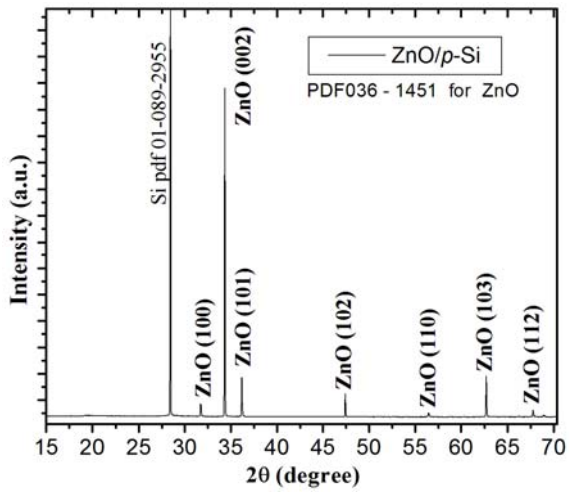

Figure 1. The X-ray diffraction pattern of the ZnO nanorods grown on *p*-Si (100) substrate.

The SEM observations of our samples (Figure 2) were in agreement with XRD data analysis (Figure 1).

Figure 2 shows a typical morphology of the ZnO nanorods deposited on *p*-Si(100) substrate. The ZnO nanorods showed grass-like morphology and the angle between nanorods and substrate plane was about 50-75°. Radius of the ZnO nanorods varied in the range 50-175 nm. The aspect ratio was estimated larger than 10.

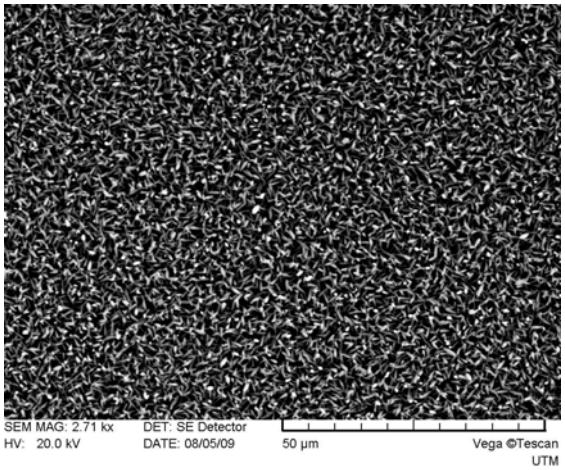

Figure 2. SEM image of ZnO nanorods hydrothermally grown on *p*-Si substrate.

Using energy dispersion X-ray spectroscopy, we found that the Zn:O ratios in our structures to be 1:1 atomic ratio in all samples.

The vibrational properties of ZnO material are important in order to understand transport properties and phonon interaction with the free carriers. Wurtzite zinc oxide belongs to $C_{6v}^4(P6_3mc)$ space group, such symmetry is one of the simplest uniaxial crystals. According to theoretical group analysis it has eight optical modes that exists at the Γ point of the Brillouin zone,

$$\Gamma_{opt} = A_1(TO,LO) + 2B_1 + E_1(TO,LO) + 2E_2$$

The two B_1 modes are silent and A_1, E_1, E_2 modes are Raman active and polar. Due to the fact that ZnO is polar along the *c* axis of its hexagonal unit cell, which is made by alternating Zn^{2+} and O^{2-} ions layers, the A_1 and E_1 modes split into TO-transverse optical and LO-longitudinal optical components. This is for four of six active modes. The remaining Raman modes are from low and high frequency submodes of E_2 which are noted as E_2(low) and E_2(high), respectively. Figure 3 shows Raman spectrum of ZnO nanorods deposited on Si(100) substrate. In the Raman spectrum can be observed distinct peaks at 99.98, 303.8, 333.4, 439.2 and 521.1 cm^{-1} in the low wave-number region. The Raman spectrum was indexed with Si and ZnO emission modes. Peaks at 303.8 and 521.1 cm^{-1} come from Si substrate (Figure 3). It can be seen a weak shoulder located at the low energy side of 439.2 cm^{-1} peak, which corresponds to E_1(TO) at 410.2 cm^{-1}. The zinc oxide peaks located at 99.98 cm^{-1} and 439.2 cm^{-1} and are attributed to the low- and high-E_2 mode respectively of non-polar optical phonons.

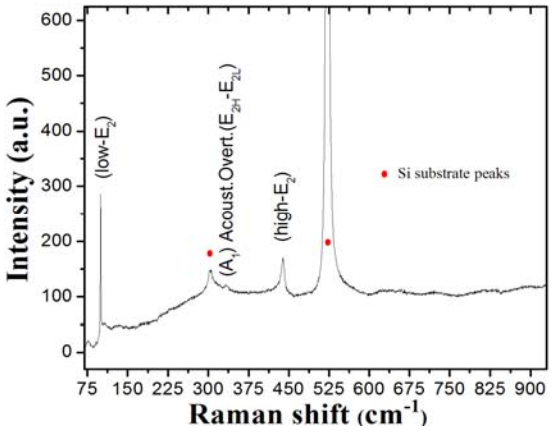

Figure 3. Room-temperature Raman spectra of ZnO nanorods hydrothermally grown on *p*-Si substrate and thermally annealed at 400 °C.

The E_2(high) is clearly visible at 439.2 cm^{-1} with a FWHM of 6 cm^{-1}, while the line-width of the peak corresponding to E_2(low) mode is about 4cm^{-1}, which is comparable to values reported for ZnO in the literature [25,28]. E_2(high) peak is associated with high sample crystallinity. In our studies, the

absence of other phonon modes indicates that all nanorods are perpendicularly quasi-oriented to the substrate surface. It can be observed that ZnO nanorods are *c*-axis oriented, which is in accordance with the SEM results presented above and XRD measurements.

Room-temperature Raman spectra of nanorods hydrothermally grown on Si substrate demonstrate the high quality of the wurtzite crystal structure of our ZnO nanomaterial.

Figure 4 shows photoluminescence (PL) spectra of the ZnO/*p*-Si structure at room-temperature. The PL spectra of the as-grown sample (Fig. 4) consist of a broad and intensive near bandgap band with the maximum at 3.26 eV at room temperature. No visible emission is observed in the sample (at least at the level three orders of magnitude less that the intensity of the near bandgap luminescence). One visible PL band at 2.38 eV can be observed in spectra, which is associated with deep levels defects in ZnO [26,28].

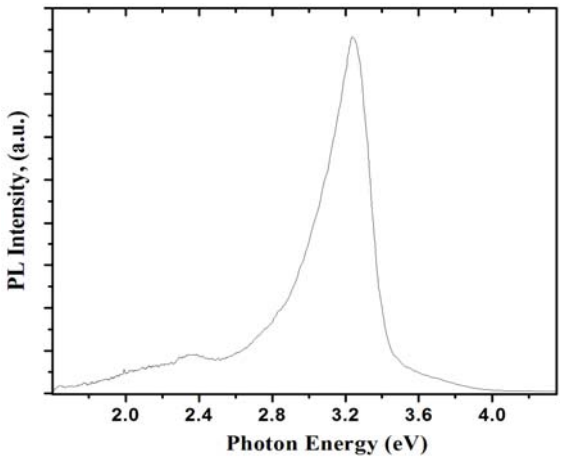

Figure 4. Photoluminescence of the *n*-ZnO-nanorods/*p*-Si structure measured at 300 K.

Figure 5 shows a typical current-to-voltage characteristic (*I-V*) curve measured in dark from as-grown ZnO/*p*-Si structure.

The *I-V* curves show rectifying properties with a turn-on voltage of ~1.2 V for forward bias and a reverse bias breakdown voltage of -3 V.

Insert in Figure 5 shows *I-V* curves (in the dark measured at 300 K) of the nano-ZnO/*p*-Si junction after annealing at 400 °C for 1 h in air.

Spectral responsivity of the ZnO nanorods/*p*-Si structure (Figure 6) and the energy band-gap model (Figure 7) were used to explain the junction formed between *n*-ZnO nanorod and *p*-Si substrate.

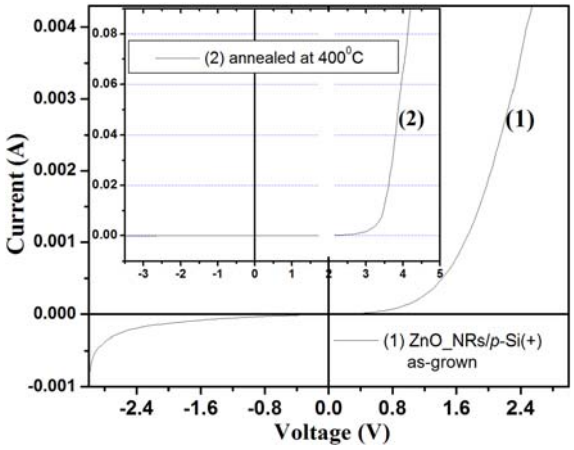

Figure 5. Typical *I-V* curve of the nano-ZnO/*p*-Si junction in the dark measured at 300 K.

Visible light photons excite charge carriers in the depletion region of the ZnO nanorods/*p*-Si junction. These excess carriers are quickly swept out to external electrodes due to the built-in electric field. Based on energy band-gap model, the depletion widths for ZnO and *p*-Si can be expressed as [27]:

$$W_{ZnO} = \left[\frac{2\varepsilon_1\varepsilon_2 N_{Si}}{qN_{ZnO}(\varepsilon_1 N_{Si} + \varepsilon_2 N_{ZnO})} V_{bi} \right]^{1/2} \quad (3)$$

$$W_{Si} = \left[\frac{2\varepsilon_1\varepsilon_2 N_{ZnO}}{qN_{Si}(\varepsilon_1 N_{Si} + \varepsilon_2 N_{ZnO})} V_{bi} \right]^{1/2} \quad (4)$$

The relative voltage supported in each semiconductor is

$$\frac{W_{ZnO}}{W_{Si}} = \frac{N_{Si}}{N_{ZnO}} \quad (5)$$

V_{bi} - the total built-in potential barrier between ZnO and *p*-Si, ε_1, ε_2 are the dielectric constants of *p*-Si and ZnO, respectively. N_{Si} is the acceptor concentration of *p*-Si (~10^{18} cm^{-3}), N_{ZnO} is the donor concentration in ZnO (about $5 \cdot 10^{15}$ cm^{-3}[28]). Thus, the ratio of depletion widths in ZnO to *p*-Si is ~200:1. In this way can be explained the detection of UV light and elimination of visible light responsivity generated in the depleted *p*-Si substrate.

The photodetection mechanism can be described by considering the optical characteristics of ZnO NRs. The energy band gap of ZnO is larger that the energy of visible photons and therefore the compound is transparent to the visible light. Thus, the visible light can pass through ZnO NRs and is absorbed by the underlying *p*-Si substrate. This

leads to generation of electron-hole ($e^- - h^+$) pairs which favor the photocurrent under reverse bias regime due to drift to ZnO region. But, the penetration depth of the light in *p*-Si is limited and leads to saturation of photocurrent. However, the UV photons are absorbed in ZnO NRs (see Figure 6) and photogenerated electrons drift to substrate electrode through the depletion region of ZnO. In this way current increases linearly with increasing the reverse voltage value (not shown).

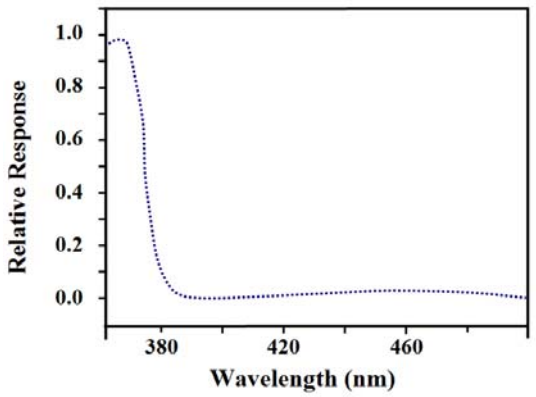

Figure 6. Spectral responsivity curve of ZnO nanorods/*p*-Si heterojunction.

To support discussions about spectral responsivity from *n*-ZnO nanorods and *p*-Si energy band diagrams were drawn. Here the effect of the interfacial state is neglected. Considering silicon dioxide layer between ZnO and *p*-Si very thin, one can neglect its effect on the energy band diagram of *n*-ZnO-nanorods/*p*-Si (Figure 7).

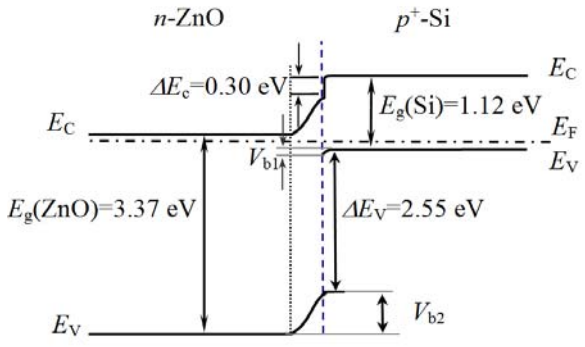

Figure 7. The schematic energy band diagram of the *n*-ZnO-nanorods/*p*-Si heterojunction structure under the equilibrium state.

Conduction band offset ΔE_C is ~ $0.30eV$ and the valence band offset are:

$$\Delta E_V = E_g(ZnO) + \Delta Ec - E_g(Si) = 2.55eV$$

In such way one can conclude that the energy barriers for holes are different than the energy barrier for electrons in ZnO/*p*-Si structures.

Electroluminescence has been observed from *n*-ZnO nanorods/*p*-Si structure at room temperature (not shown) when a positive voltage is applied to the *p*-Si/In-Ga substrate accordingly to a similar schematic representation like in Ref [7]. In our experiments no emission was observed under reverse bias of *p*-*n* heterojunction. Under forward bias of the structure white emission prove to dominate the electro-luminescence spectra.

4. CONCLUSION

In summary, ZnO nanorod arrays on *p*-type Si heterostructures were synthesized via catalyst-free hydrothermal route without template. The heterostructures consist of high-quality ZnO nanorods confirmed by SEM, XRD, Raman and photoluminescence studies. These characterizations demonstrate that the ZnO material is composed from one-dimensional nanorods with good crystal quality and *c*-axis quasi-oriented to *p*-type Si substrate. The results are consistent with the nanocrystalline nature of the zinc oxide material as observed in SEM, XRD and Raman data. It is discussed the spectral responsivity from *n*-ZnO nanorods and *p*-Si based on energy band diagrams and explain main points of the photodetection mechanism in such heterostructures.

Presented data substantially contribute to overcome some obstacles in uses of nanorods/nanowires for further development of the device structures. Also have been satisfied the features of the nanowire synthesis method desired for industry such as low-cost materials and processing, control of process parameters, environment friendly reagents, etc.

Further work: Our further research efforts are directed towards finding an optimum deposition regime for an optimum ZnO/*p*-Si interface where a very thin SiO_2 layer is formed after deposition. Also, efforts are directed towards synthesizing oriented one – dimensional nanorods, which will facilitate construction of semiconductor nanodevices with well-ordered alignment, expected to be extremely important for scientific, technological and industrial applications. Development of single doped ZnO nanorod/*p*-Si LED was addressed as well.

Acknowledgements. Author would like to acknowledge Professors I.Tighineanu, Th.Pauporté and L.Chow for their guidance of my post-doctorate

research in their laboratories in Moldova, France and U.S.A., respectively. Also, their enormous support of all performed scientific research and detailed discussions of the experimental data are gratefully acknowledged.

References

1. H. Brown, *J. Phys. Chem. Solid. 15, p. 86, 1960.*

2. O. Lupan, T. Pauporté, B. Viana, I.M. Tiginyanu, V.V. Ursaki, R. Cortés, *Epitaxial Electrodeposition of ZnO Nanowire Arrays on p-GaN for Efficient UV-Light Emitting Diode Fabrication. ACS Appl. Mater. Interfaces 2, p. 2083-2090, 2010.*

3. D.J. Rogers, F.H. Teherani, A. Yasan, K. Minder, P Kung, M. Razeghi, *Appl. Phys. Lett. 88, p. 141918, 2006.*

4. X. Wang, Q. Li, Z. Liu, J. Zhang, Z. Liu, R. Wang, *Appl. Phys. Lett.* ***84****, p. 4941, 2004.*

5. M.H. Huang, S. Mao, H. Feick, H.Q. Yan, Y.Y. Wu, H. Kind, E. Weber, R. Russo, P.D. Yang, *Science 292, p. 1897, 2002.*

6. M. Willander, O. Nur, Q.X. Zhao, L.L. Yang, M. Lorenz, B.Q. Cao, J. Zúñiga Pérez, C. Czekalla, G. Zimmermann, M. Grundmann, A. Bakin, et al.*, Nanotechnology 20, p. 332001, 2009.*

7. O. Lupan, T. Pauporté, B. Viana, *Low-voltage UV-Electroluminescence from ZnO-Nanowire Array/ p-GaN Light Emitting Diodes, Advanced Materials, 22, p. 3298-3302, 2010.*

8. O. Lupan, G. Chai, L. Chow, *Microelectronic Eng. 85, p. 2220, 2008.*

9. H. Ohta, K. Kawamura, M. Orita, M. Hirano, N. Sarukura, H. Hosono, *Appl. Phys. Lett. 77, p. 475, 2000.*

10. A. Tsukazaki, A. Ohtomo, T. Onuma, M. Ohtani, T. Makino, M. Sumiya, K. Ohtani, S.F. Chichibu, S. Fuke, Y. Segawa, H. Ohno, H. Koinuma, M. Kawasaki, *Nature Mater. 4, 42, 2005.*

11. Y.I. Alivov, D.C. Look, B.M. Ataev, M.V. Chukichev, V.V. Mamedov, V.I. Zinenko, Y.A. Agafonov, A.N. Pustovit, *Solid-State Electron. 48, p.2343, 2004.*

12. **S.Y. Liu,** ***T. Chen, Y.L. Jiang, G.P. Ru, X.P. Qu,*** *J. Appl. Phys. 105, p. 114504, 2009.*

13. K.Y. Lo, S.C. Lo, C.F. Yu, T. Tite, J.Y. Huang, Y.J. Huang, R.C. Chang, S.Y. Chu, *Appl. Phys. Lett. 92, p. 091909/1, 2008.*

14. B.M. Kayes, H.A. Atwater, N.S.J. Lewis, *Appl. Phys. 97, p. 114302/1, 2005.*

15. **A. Miyake,** ***H. Kominami, H. Tatsuoka, H. Kuwabara, Y. Nakanishi, and Y. Hatanaka,*** *J. Cryst. Growth 214-215 p. 294, 2000.*

16. A. Nahhas, H. Koo Kim, J. Blachere, *Appl. Phys. Lett. 78, p. 1511, 2001.*

17. K. Iwata, P. Fons, S. Niki, A. Yamada, **K. Matsubara,** **K.** ***Nakahara, T. Tanabe, H. Takasu,*** *J. Cryst. Growth 214-215, p. 50, 2000.*

18. M. Watanabe, Y. Maeda, S. Okano, *Jpn. J. Appl. Lett 39, p. 500, 2000.*

19. C. Shaoqiang, Z. Jian, F. Xiao, W. Xiaohua, L. Laiqiang, S. Yanling, X. Qingsong, W. Chang, Z. Jianzhong, Z. Ziqiang, *Applied Surface Science 241, p. 384-391, 2005.*

20. K. Ogata, S. -W. Kim, Sz. Fujita, Sg. Fujita, *J. Cryst. Growth 240, p. 112-116, 2000.*

21. Silicon Solar Cell Material and Technology*, Springer Berlin, Heidelberg, Vol. 112, Book "Photovoltaic Solar Energy Generation", p. 23-41, 2000.*

22. V. Lehmann*, Electrochemistry of Silicon: Instrumentation, Science, Materials and Applications, Wiley-VCH Verlag GmbH D-69469 Weinheim, 2002.*

23. W.A. Kem, D.A. Puotinen, *RCA Rev. 31, p.187, 1970.*

24. O. Lupan, L. Chow, G. Chai, B. Roldan, A. Naitabdi, A. Schulte, H. Heinrich, *Nanofabrication and characterization of ZnO nanorod arrays, Materials Science and Engineering, B 145 p. 57, 2007.*

25. O. Lupan, V.V. Ursaki, G. Chai, L. Chow, G. Emelchenko, I.M. Tiginyanu, A.N. Gruzintsev, A.N. Redkin, *Selective hydrogen gas nanosensor using individual ZnO nanowire with fast response at room temperature. Sensors and Actuators B: Chemical, 144, nr.1, p. 55-66, 2010.*

26. V.V. Ursaki, I.M. Tiginyanu, V.V. Zalamai, V.M. Masalov, E.N. Samarov, G.A. Emelcenko, F. Briones, *Photoluminescence of ZnO layers grown on opals by chemical deposition from zinc nitrate solution, Semiconductor Science and Technology, 19, p. 851-854, 2004.*

27. S.M. Sze, *Physics of Semiconductor Devices, 2 ed., Wiley, New York, 1981, p.124, 1981.*

28. I.M. Tiginyanu, O. Lupan, V.V. Ursaki, L. Chow, M. Enachi, *Nanostructures of Metal Oxides. Comprehensive Semiconductor Science & Technology (SEST), Encyclopedia - edited by S. Wood, R. Fornari, and Hiroshi Kamimura, pp. 396-479, 2011.*

Recommended for publication: 25.05.2011